Tutor

Dr. Francesc Viñes Solana
Departament de Ciència de Materials i Química Física

Grau de Química

Treball Final de Grau

Coinage and Pt-Group Metal Surfaces Stability
Estabilitat de Superfícies de Metalls Encunyables i del Grup del Pt

Judit Ruvireta Jurado

June 2016

Universitat de Barcelona

B:KC Barcelona Knowledge Campus
Campus d'Excel·lència Internacional

Què és la felicitat, sinó el desenvolupament de les nostres facultats?

Germaine Necker

Si ja és prou complicat escriure un TFG de Química computacional, ara toca expressar els agraïments envers tota la gent que m'ha ajudat a tirar endavant aquest estudi. Començar per la meva companya i amiga Lorena Vega que juntament nostre tutor Francesc Viñes, han fet d'aquest extens estudi quelcom divertit tot i les inconveniències. Agrair sobretot les moltíssimes hores de dedicació d'en Francesc Viñes, que m'han permès entendre una mica més la complicada química teòrica i d'aquest manera veure un altre vessant de la recerca química. Donar les gràcies també a totes les amistats i familiars que m'han donat suport a tirar endavant en moments més estressants. Sense cap d'ells no hagués estat possible tot el camí recorregut. En serio, moltes gràcies.

REPORT

CONTENTS

1. SUMMARY

Coinable (Cu, Ni, Ag, Au) and Pt-group metals (Pt, Pd, Ir, Rh) are face centered cubic (*fcc)* transition metals used in catalysis as active phases, usually in the form of nanoparticles. These nanoparticles mostly expose most stable surfaces, which are the main responsible of the interaction with reagents.

Here we studied, by Density Functional Theory (*DFT*) calculations using slab models, the surface stability, in terms of surface energy, relaxation, degree of compression, and coordination number. The most stable surfaces studied are those with higher degree of compression and lowest Miller index, such as (111), (011), and (001) surfaces, which *a priori* are the most stable ones. Results were obtained, comparing and commenting two levels of computation, either using the Perdew-Burke-Ernzerhof (*PBE*) or the Tao-Perdew-Staroverov-Scuseria (*TPSS*) exchange-correlation functionals.

The results suggest that the surface energy shows the typically parabolic dependence on the *d* band occupation in transition metals. It is also found that (111) surface is the most stable one because of its higher degree of compression, lower energy relaxation and surface energy. Furthermore, TPSS functional gives better surface energies with higher accuracies yet the data are more difficult to obtain. In contrast, semi-empirical methods can only be used for qualitative studies as they are just good giving trends of surface energy.

Keywords: Surface energy, *fcc* transition metals, stability, slab model, density functional theory

2. RESUM

Els metalls encunyables (Cu, Ni, Ag, Au) i els metalls del grup del Pt (Pt, Pd, Ir, Rh) són metalls de transició *fcc* emprats en catàlisi com a fases actives, normalment en forma de nanopartícules. Aquestes nanopartícules exposen principalment les superfícies més estables, que són les responsables de la interacció amb reactius.

En aquest treball de fi de grau s'ha estudiat la estabilitat de les superfícies amb Índex de Miller més baixos – (001), (011), i (111) –, que son les més compactes, i per tant, *a priori*, les més estables. L'estabilitat és mesurada en funció de la energia superficial, el grau de compactació de la superfície, el nombre de veïns i la relaxació superficial. Aquestes dades s'han obtingut realitzant càlculs computacionals basats en la teoria del funcional de la densitat (Density Functional Theory – DFT) i emprant un paquet de càlcul amb condicions periòdiques de — Viena *Ab Initio* Simulation Package – VASP — i model de llesca (*slab*). S'han comparat dos funcionals adients en la descripció del interior (*bulk*) dels metalls de transició, el de Perdew-Burke- Ernzerhof (*PBE*), i el de Tao-Perdew-Staroverov-Scuseria (*TPSS*).

Els resultats suggereixen que l'energia superficial segueix un dependència parabòlica amb la ocupació dels orbitals *d* dels metalls de transició. També s'ha corroborat que la superfície més estable és la (111) ja que és la més compacte i amb la que s'obtenen menors energies de relaxació. A més, s'ha trobat que emprant funcional TPSS les energies superficials calculades amb regressió lineal són les que tenen més precisió, tot i el seu elevat cost computacional, comparant amb el funcional PBE. Per altre banda, els mètodes semi-empírics només es poden emprar per estudis qualitatius degut que només són correctes definint les tendències de l'energia superficial.

Paraules clau: Energia superficial, metalls de transició *fcc*, estabilitat, model de *slab,* teoria del funcional de la densitat

3. INTRODUCTION

Metals have such interesting properties that make them ideal materials for a diverse range of applications, and so they are widely used in industry, electronics, catalytic converters, thermocouples, fuel cells, in petroleum refining, and numerous laboratory equipments.

The metal properties raise from the metallic bond and the crystallographic structure. The metallic bond is to date fully understood by molecular orbital and band theories and the properties raise as a result of the electron delocalization in the metallic bonding where an electron cloud surrounds the atoms.[1] Concerning the atomic position, most of transition metal atoms arrange in one of the following crystallographic structures; the body-centred cubic (*bcc*), the face-centred cubic (*fcc*), or the hexagonal close-packed (*hcp*) structures; see Fig. 1.

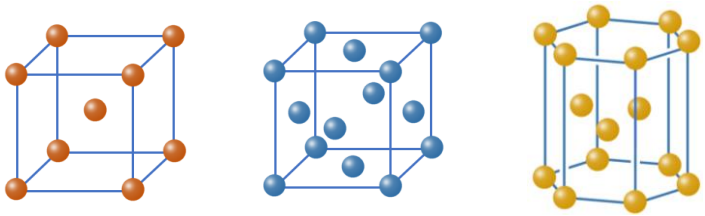

Figure 1. The *bcc* (left), *fcc* (middle), and *hcp* (right) crystallographic structures. Coloured spheres denote metal atoms.

Both *fcc* and *hcp* are close-packed structures, and the main difference between them is the layer stacking, *hcp* has an ABA stacking whereas *fcc* has an ABC stacking, see Fig. 2.

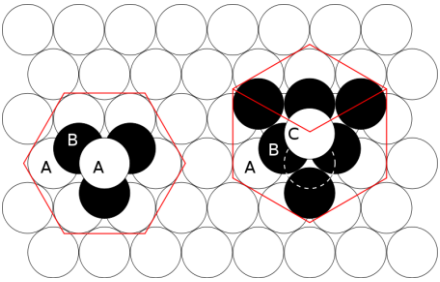

Figure 2. The *hcp* (left) and *fcc* (right) stacking along *fcc* [111] low Miller indices direction.

Here we focus on *fcc* transitional metals, which are actually the so-known coinage metals Cu, Ni, Ag, and Au, and the Pt-group Pt, Pd, Ir, and Rh metals. They are used not only for coins or jewellery, but also most used in heterogeneous catalysis as active phases, typically in the form nanoparticles supported on an inert oxide with high surface area, yet other supports, such as carbides, are becoming appealing.[2] These nanoparticles tend to mostly expose those surfaces with highest stability, which are then the main responsible of the interaction of the catalyst with reagents, intermediates, and products.

The exposure of one or another surface is determined by the surface stability, ruled by the so-called surface energy, *i.e.* the energy necessary to create the flat surface. Surface energies are fundamental in understanding a wide range of surface phenomena including growth rate, crystallite processes, grain boundaries formation, sintering processes, the catalytic performance, atomic or molecular adsorption/desorption, surface segregation, passivation, corrosion, relaxation, and reconstruction processes. [3]

The experimental determination of surface energies is very challenging; high temperatures are needed to measure surface tension changes at the metal melting temperature and values extrapolated to lower temperatures.[4] Moreover, experimental determination of a specific surface plane is extremely rare. However, the surface energy effects, like predominance of certain planes, are easily observed with microscopy techniques, and oftentimes macroscopically featured in mineral crystallites. However, surface energy can be relatively easily calculated with theoretical methods, Density Functional Theory (*DFT*) being the working horse, and thus, an effective mean to get reasonable estimates, at least for trends, which help at rationalizing the above-mentioned phenomena.

The most interesting surfaces to explore are those with the lowest energy,[5] which tend to be the close-packed surfaces with low Miller indices, such as the (111), (011), or (001) surfaces for *fcc* metals, the ones here studied. We assess different ways of estimating surface energies at two levels of computation within DFT; either using the Perdew-Burke-Ernzerhof (*PBE*) or the Tao-Perdew-Statoverov-Scuseria (*TPSS*) exchange-correlation functionals, thus comparing their suitability. The stability is studied as a function of bulk cohesion, surface compactness, and degree of saturation, accounting as well the surface relaxation and the relaxation energy once the surface is created. Semi-empirical methods are also studied to size their accuracy.

4. OBJECTIVES

The overall aim of this project is to study the energetic stability and structure of the possible low Miller indices surfaces of *fcc* transition metals. The specific objectives are:

- To model most stable (001), (011), and (111) surfaces of *fcc* metals with slab models of variable width.
- To compare and calculate the surface energies at two levels of computation within DFT; using either the PBE or the TPSS exchange-correlation functionals, assessing their suitability comparing to available experimental data.
- To estimate de degree of surface relaxation, comparing PBE and TPSS structural data with experimental values.
- To estimate surface energy dependence on the surface compactness, saturation, relaxation energy, and bulk cohesive energy.
- To assess various semi-empirical models to estimate surface energies, either using Stephan equation or the broken-bond model.
- To unravel the *fcc* transition metal surfaces stability obtaining trends along groups and series, and the implication in nanoparticle catalysts.

5. METHODS

5.1. SCHRÖDINGER EQUATION AND HARTREE-FOCK

Quantum chemistry methods are based on the resolution of the Schrödinger equation to obtain a system energy (E) using a Hamiltonian operator ($\hat{H}$), which includes the kinetic contribution of the electrons ($\hat{T}_{elec}$) and the atomic nuclei ($\hat{T}_{nuc}$), the potential interaction between them ($\hat{V}_{elec-nuc}$), and between electrons ($\hat{V}_{elec-elec}$) and nuclei ($\hat{V}_{nuc-nuc}$).[2] This Hamiltonian can be written in one simple line:

$$\hat{H}\Psi = E\Psi \qquad \text{(Eq. 1)}.$$

Within the Born-Oppenheimer approximation the equation becomes:

$$\hat{H}_{elec}\Psi = \left(\hat{T}_{elec} + \hat{V}_{elec-elec} + \hat{V}_{elec-nuc}\right)\Psi \approx E\Psi \qquad \text{(Eq. 2)}.$$

Thus the Born-Oppenheimer approximation lies in decoupling electronic and nuclear movements, knowing that the relative mass of nuclei is much higher than the electron ones. As a result, the kinetic energy of electrons does not depend on the nuclei movements, the kinetic energy of nuclei is assumed zero, and the interaction between nuclei is a constant determined given a nuclear configuration. Then one only needs to solve the electronic Hamiltonian, $\hat{H}_{elec}$.

A simple method to obtain an approximation of the energy for a polielectronic system is the Hartree-Fock (*HF*). This variational method uses just one Slater determinant, made of monoelectronic spinorbitals. Although HF method does not introduce the electronic correlation between electrons with different spin, it is a good first approximation and it opens the door to other methods with more precision, which account for correlation energies, known as post-HF methods.

The main disadvantage of HF and post-HF methods is that they cannot be used to study large and complex systems due to its high computational cost. Nevertheless, the revolution of computational chemistry of recent years has been DFT, which is detailed next.

5.2. DENSITY FUNCTIONAL THEORY

Methods based on electronic density functionals,[2] also known as DFT, are an alternative to *ab initio* traditional methods, which are based on wavefunctions. DFT is the most popular theoretical approach nowadays available for solving the electronic structures of solids and their surfaces in general, and so for metal surfaces.

The main advantage of DFT methods is that they are much more economic from the computational point of view, because the electronic density function has only three variables (four counting spin), whereas wave function depends on 3N variables for an N electrons system. Moreover, DFT permits to introduce correlation and exchange energies, although many approximations are needed for so, and so different DFT methods have been developed with increasing precision.

The electronic density function describes the number of electrons found in a differential volume *dr* with arbitrary spin. Then, the total space integral of $\rho(r)$ gives the total number of electrons of the system, where electronic density is zero at infinite distance for an isolated non-periodic system.

$$\int \rho(r)\, dr = N \qquad \text{(Eq. 3)}$$

$$\rho(r \to \infty) = 0 \qquad \text{(Eq. 4).}$$

Hohenberg and Kohn established the ground of DFT basis, which was later finalized with the Kohn-Sham method, see next.

5.2.1. Hohenberg-Kohn theorems

5.2.1.1. First Hohenberg-Kohn theorem

The first Hohenberg-Kohn (*HK*) theorem shows that two electronic systems with external potentials that differ by more than a constant cannot have ground states with the same electron density.[2] In other words, the electronic density of a system is specific to a given external potential, and *vice versa*.

$$\rho(r) \to V_{ext}(r) \quad ; \quad V_{ext}(r) \to \rho(r) \qquad \text{(Eq. 5).}$$

5.2.1.2. Second Hohenberg-Kohn theorem

The second HK theorem states that there cannot be two different systems with the same electronic density in its fundamental state. The energy is a universal functional of the electronic density, then

$$E = E[\rho(r)] \geq E_0 = E[\rho_0(r)] \quad \text{(Eq. 6).}$$

5.2.2. Kohn-Sham method

The last decisive step to develop DFT was the Kohn-Sham (*KS*) so-known formalism.[2 6] The authors pointed that a polielectonic system described with a density ρ(r) can be related to another system made of non-interacting electrons with the same density ρ(r) called the Jellium model, and in this way ρ(r) can be expressed as que sum of squared monoelectronic N spinorbitals ϕ_i, called KS orbitals. At practice ϕ_i of Jellium are similar to monoelectronic orbitals, and can be as well expressed as a function of other functions basis-set.

$$\rho(r) = \rho_{KS}(r) = \sum_{i=1}^{N} |\phi_i(r)|^2 \quad \text{(Eq. 7).}$$

5.2.3. Exchange and correlation functionals

Within KS method, all different contributions to the system energy are known, but the exchange and correlation energy.[2 5] The exchange and correlation functional is the key for the correct application of DFT. Within the Born-Oppenheimer approximation, the theory is exact. However, the precise form of $E_{XC}[\rho]$ is unknown, yet can be divided into two terms; the electron exchange and the electronic correlation.

$$E_{XC}[\rho] = E_X[\rho] + E_C[\rho] \quad \text{(Eq. 8).}$$

The electron exchange emerges because a many-body wavefunction must be antisymmetric under the exchange of any two electrons with same spin. This antisymmetry of the wavefunction is simply a general expression of the Pauli exclusion principle, but reduces the Coulomb energy of the electronic system by increasing the spatial separation between electrons of same spin. The electron correlation further reduces the Coulomb energy between electrons of different spin because the motion of each individual electron is correlated with the motion of all others, helping also to keep electrons of odd spin spatially separated. Next some well-known approximations for the exchange and correlation functional are detailed.

5.2.3.1. Local density approximation

The Local Density Approximation (*LDA*) is the simplest approximation to get the exchange and correlation functional and it is based on the assumption that the electron density does not change much with the position, and so depends *only* on the position. Then, the exchange-correlation density can be taken as that of a uniform electron gas of same density.[2 5]

Modern LDA functionals tend to be exceedingly similar, differing only in how their correlation contributions have been fitted to a many-body free electron gas data. The Perdew-Zunger (*PZ*), Perdew-Wang (*PW)*, Ceprley-Alder (*CA*), and Vosko-Wilk-Nusair (*VWN*) functionals are all common LDA functionals. Despite its simplicity, LDA can give good results for systems with slow varying densities such as atoms, molecules, solids, and surprisingly, good results for metal surfaces.

5.2.3.2. Generalized gradient approximation

To improve LDA approximation density gradients are included in the exchange-correlation functional. This is the so-known Generalized Gradient Approximation (*GGA*). The most widely used GGAs in solid state physics are Perdew-Wang *(PW91*), and PBE. PBE actually got several offspring; rev-PBE, RPBE, PBE-WC, and PBEsol. The so-called meta-GGA consider density gradients and laplacians in their formulas being, either TPSS and revTPSS are examples. In this work PBE and TPSS exchange correlation functionals are the ones contemplated.[2 5]

5.2.3.3. Hybrid functionals

Hybrid functionals use a part of the exchange energy from HF method, plus part of exchange and the full correlation from LDA or GGA methods. Becke-Lee-Yang-Parr (*B3LYP*) functional is probably the most common hybrid functional used in the quantum chemistry community, given its great performance on molecular thermochemistry.

5.3. PERIODIC SOLIDS

Crystalline solids have, by definition, periodicity. This periodicity introduces important elements of simplicity when representing solids to obtain important information of their chemical and physical behaviour, for either chemical, physical, or catalytic applications. The Schrödinger equation or electron density can be solved for just a small unit cell with periodic boundary conditions and so avoiding to do so for the whole solid structure. Bloch theorem states that the wavefunction cannot be affected when it is moved to an equivalent point of a replicated cell, and so all its properties are then intrinsically periodic. [2]

5.3.1. Crystalline structures

The perfect arrangement and periodic structure of the atoms of a crystalline solid at 0 K is the key to reproduce the totality of the solid. The part of the solid which is transitionally repeated is called the unit cell and it is used to study the properties of the bulk. Depending on the lattice vectors and positions of the atoms inside the unit cell we can have different arrangements. The *fcc* structure is the one studied in this work. It is considered a close-packed structure with a coordination number in the bulk of twelve, and four atoms per cell, see Fig. 3.

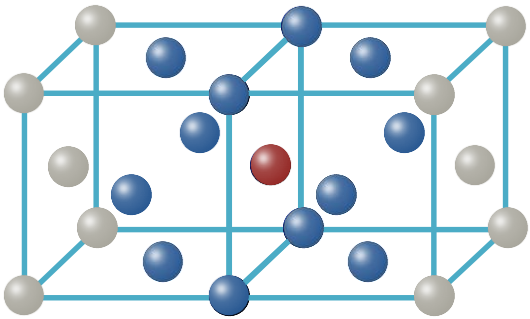

Figure 3. The *fcc* coordination number. Light blue spheres denote the 12 atoms surrounding the red atom.

5.3.2. Reciprocal space and k-points

The essential characteristic of metallic bond is that the valence electrons are delocalized among a lattice of metal atoms. Delocalization is the consequence of a heavy overlap between the individual valence wavefunctions resulting in the valence electrons being shared by all the atoms in the metal. Then, atoms can be perceived as atomic nuclei immersed in a sea of electrons. This electron sea leads to a bonding that is generally not directional, resulting in close-packed crystal structures being often favoured. Because of the strong overlap of the orbitals the resulting electronic wavefunction or bands of a metal will thus exhibit a strong dispersion in reciprocal space, also called **k**-space or first Brillouin zone.

Reciprocal space is an alternative space of the real space in the Bravais lattice, which is useful for studying solids. It can be defined for its lattice vectors b_i, which are related with the real lattice vectors a_i of the cell as seen in Eq. 9 and exemplified in Fig. 4.

$$b_i = 2\pi \frac{a_j \times a_k}{a_i \cdot (a_j \times a_k)} \quad \forall_{i,j,k} \in \{1,2,3\} \qquad \text{(Eq. 9).}$$

$$a_i \cdot b_j = 2\pi \delta_{ij} \qquad \text{(Eq. 10).}$$

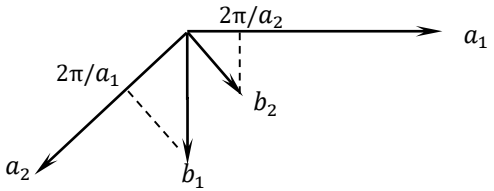

Figure 4. Reciprocal and real space vectors.

To simplify the study of the reciprocal space, we can take advantage of symmetry elements. Therefore, one just needs to study a discrete number of lattice vectors **k**, also called **k**-points. In practice, a Monkhorst-Pack grid of **k**-points is used and a thinner grid is used when convergence of an observable, such as energy, is reached. Finally, note that the reciprocal space volume reduces as the real space increases. A big grid is needed for small unit cells and only a **k**-point for cells with a large volume.

5.3.3. Pseudopotentials

Pseudopotentials are used because of the high computational cost of systems with many electrons, such as transition metals. The idea is that the core electrons of an atom result unaffected when there is a chemical change in the surroundings of the atom. This way, the effect of core electrons can be joined to an effective potential assuming that the core electrons do not change at all. This results in decreasing the number of plane-wave functions because core electrons are not explicitly described, so valence electrons, which are the main responsible of the chemical processes, are the only ones studied.

The Projector Augmented Wave (*PAW*) method was developed by Blöchl[7] in 1994 and permits to describe with precision core electrons, resembling an all-electron calculation. PAW method pretends to solve the problem by dividing the wavefunctions in to two regions, one soft reacting region and another for core electrons. In this work, PAW pseudopotencials are used.

5.3.4. Slab model

Bloch theorem can be applied for surfaces, allowing the electronic structure problem for infinite 3D solids to be used in 2D simulations. This is done by introducing a vacuum region along the studied surface normal direction, see examples in Fig. 5.

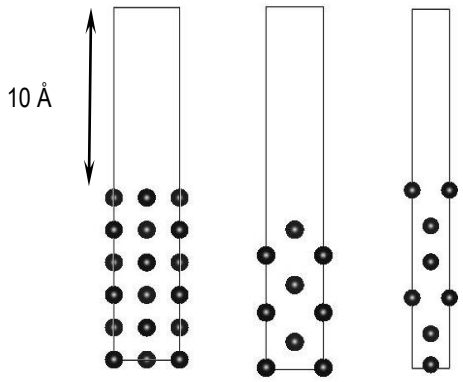

Figure 5. Six-layer slab stacking along [001] Miller index direction (left), [011] (middle), and [111] (right) for an *fcc* transition metal with 10 Å of vacuum. Black spheres denote metal atom positions.

The periodic boundary conditions ensure these slabs to be infinite along surface plane, but also normal to it, where the 10 Å vacuum repeats infinitely. The slab model implies studying different number of layers to obtain the correct description of electronic properties of a metallic surface. Therefore, in the present work, thickness as of 4, 5, and 6 layers have been studied to obtain convergence of surface energy of *fcc* metals cut perpendicular to [001], [011], and [111] Miller indices directions.

5.4. SURFACE ENERGY

Surface energy is probably the main energetic feature of surfaces and it is one of the basic quantities to understand the surface structure, reconstruction, roughening, and relaxation. Cleavage energy can be defined as the energy required to split an infinite crystal into two parts, given per surface area. When two identical surfaces are created, the cleavage energy equals two equivalent surface energies.

Despite its importance, the experimental value of surface energy is difficult to determine. Most of the experiments are performed at high temperatures where the surface tension of the liquid is measured, which is then extrapolated to 0 K. Moreover, these experiments contain certain uncertainties such as that surface energy values belong to an isotropic crystal. Therefore, a theoretical determination discerning different surface endings is of vital importance. Recently surface energy of metals has been calculated using *ab initio* techniques with unprecedented accuracy. Surface energy is calculated in this work in four different ways, two *ab initio*, and two using semi-empirical equations; the Stephan equation or the broken-bond model.[3 8]

The first *ab initio* method is to calculate surface energy by knowing that it can be defined as the energy, per unit area, required to form two equivalent surfaces by splitting a bulk crystal into two parts, and it can be written as:

$$\gamma_{relax} = \frac{E_{slab} - N\, E_{bulk}}{2\, A} \qquad \text{(Eq. 11)}$$

where E_{slab} and E_{bulk} are the total energies of the slab and the crystal bulk, respectively, N is the number of atoms composing the slab unit cell, and A is the surface area of each of two equivalent exposed surfaces.

Another method is derived from a readjustment of Eq. 11 and a linear regression of E_{slab} versus N obtaining the surface energy at the equation intercept:

$$E_{slab} = N\,E_{bulk} + 2\gamma_{relax}A \quad \text{(Eq. 12).}$$

Within this methodology, a set of slabs with different thickness, from 4 to 6 layers, has been considered to perform a linear regression of E_{slab} as a function on N. Note that slope should be E_{bulk}.

When using Stephan semi-empirical equation[9] some parameters are needed, which are the vaporisation enthalpy ΔH^{o}_{vap}), the molar mass (M), the density of the metal (ρ), and the coordination numbers of the slab (Z_s) and bulk (Z):

$$\gamma = \frac{\Delta H^{o}vap\ \ \rho^{2/3}}{M^{2/3}\ \ {N_A}^{1/3}}\ \ \frac{Z_S}{Z} \quad \text{(Eq. 13).}$$

On the other side, the traditional semi-empirical broken-bond model[10 11 12] is used as well to estimate surface energy values at T = 0 K for the transition metals with different facets. Since the bond strength becomes larger for an atom with a smaller coordination number, this coordination number bond strength relation can be quantified using the tight-binding approximation. Knowing that the total crystalline energy is a sum of contributions of all bonds of an atom, surface energy can be estimated as the energy per bond assumed to scale with squared coordination number leading to the next equation:

$$\gamma = \frac{\sqrt{Z}-\sqrt{Z_S}}{\sqrt{Z}}\ \ E_{coh} \quad \text{(Eq. 14).}$$

Note that both semi-empirical methods assume a dependence with Z_s, but to a different extent, and, in adidition a direct proportionality to the metal cohesion quantified as ΔH^{o}_{vap} and E_{coh}, respectively.

6. COMPUTATIONAL DETAILS

The DFT calculations have been performed using the Vienna *Ab Initio* Simulation Package (*VASP*) and PAW pseudopotentials. The electronic exchange-correlation was described by PBE GGA and TPSS metaGGA functionals. Valence electron density was expanded in a plane-wave basis set with a 415 eV cutoff energy for the kinetic energy. A standard slab structure was used to model the surface systems, containing 4, 5, or 6 layers for (001), (011), and (111) surface orientations. All atoms were allowed to relax during optimizations. These optimizations have been carried out using the tetrahedron smearing method with an energy width of 0.2 eV to speed up convergence, yet final energies are extrapolated to 0K (no smearing).

The electronic structure calculations were non spin-polarized, with the exception of the isolated metal atoms and Ni systems. An optimal Morkharst-Pack grid of 7×7×7 special **k**-points dimensions was found to be sufficient for accurate bulk total energy calculations in most stringent metals —shortest cell parameters—, and so used for all bulk calculations.

When computing atoms in vacuum, a broken symmetry cell of 9×10×11 Å dimensions was employed to ensure proper occupancy of degenerate orbitals. These atomic optimizations have been carried out using a Gaussian smearing with an energy width of 0.001 eV in order to have the correct population in each orbital. Given the isolated character of atoms, calculations were carried out at **Γ**-point.

In the case of slab calculations, a 7×7×1 Morkharst-Pack grid was used to sample the reciprocal space. Bulk and slab optimizations were stopped when atomic forces acting on atoms were below 0.02 eV $Å^{-1}$, and an electronic convergence criterion of 10^{-6} eV was used.

7. RESULTS

7.1. BULK

Bulk calculations were done to ascertain whether bulk has been described with a sufficiently correct degree of accuracy. For these calculations, cohesive energy and the shortest interatomic distances (δ) were obtained and compared with previous PBE and TPSS calculations and experimental data. Cohesive energy of *fcc* metals was calculated as the difference between the energy per atom in bulk ($\frac{E_{bulk}}{N}$) and the energy of an isolated atom, E_{at}, see Eq. 15.

$$E_{coh} = E_{at} - \frac{E_{bulk}}{N} \qquad \text{(Eq. 15).}$$

Comparing calculated values with experimental ones, there is very good agreement with PBE functional but TPSS only captures trends, see Table 1. The poorer accuracies of TPSS calculations are due to its difficulty in describing isolated atoms.

Metal	$E_{coh}^{exp.}$ [a]	E_{coh}^{PBE} [b]	E_{coh}^{PBE}	E_{coh}^{TPSS} [b]	E_{coh}^{TPSS}
Ni	4.48	4.87	4.84	5.40	6.12
Cu	3.51	3.48	3.48	3.73	4.45
Rh	5.76	5.62	5.61	6.22	6.73
Pd	3.93	3.71	3.70	4.01	4.00
Ag	2.96	2.49	2.48	2.73	3.29
Ir	6.96	7.32	7.35	7.71	7.73
Pt	5.87	5.50	5.49	5.79	5.43
Au	3.83	2.99	2.98	3.28	3.30

(a) Ref. 13, (b) Ref. 14.

Table 1. Cohesive energy calculated within PBE and TPSS functionals and experimental values. All data is given in eV/atom.

A way to quantify the accuracy of these methods is by calculating the Mean Error (*ME*) and the Mean Average Error (*MAE*). Then, one can see that TPSS overestimates the cohesive energy values and that PBE is better suited, see Table 2 below.

Error	PBE		TPSS	
	Exp.	PBE	Exp.	TPSS
ME	-0.17	-0.01	0.47	0.27
MAE	0.36	0.01	0.71	0.37

Table 2. ME and MAE of cohesive calculations.

Although TPSS values of cohesive energies are not as good as PBE ones, TPSS functional give results with similar accuracy for the calculated shortest interatomic distances in bulk, see Figure 6. For Ni and Cu bulk calculations, however, there is slight deviations to experimental ones. The shortest interatomic distance within a crystal cell, δ, depends on the lattice parameter **a**, which in the *fcc* structure, it equals **a**/√2.

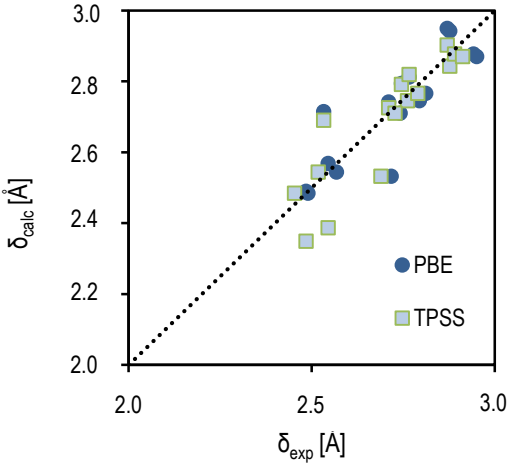

Figure 6. Calculated δ, δ_{calc}, versus experimental values, δ_{exp}. Dotted line would represent perfect agreement.

7.2. SURFACE RELAXATION

The surface relaxation (atomic movement in the surface normal direction) observed in the calculations is based on the fact that atoms at the surface of a crystal have less neighbours than they do in the bulk, and so they are then under-coordinated, as the electronic readjustment makes that they do not remain at their precise *bulk truncated* positions. Rather, the few atoms from the top layers of the metal are likely to move, retaining their periodicity, in response to their new environment. So, when a crystal is cut to form a surface, atoms rearrange in order to reduce the charge-density corrugations. This leads to a motion of the atoms left on top of the surface atoms resulting in a displaced position towards the rest of the crystal. This is schematically illustrated in Fig. 7 (where $d_{12} = d_{34}$ and $d_{12} < d_{23}$ as a result of symmetric layer relaxation).

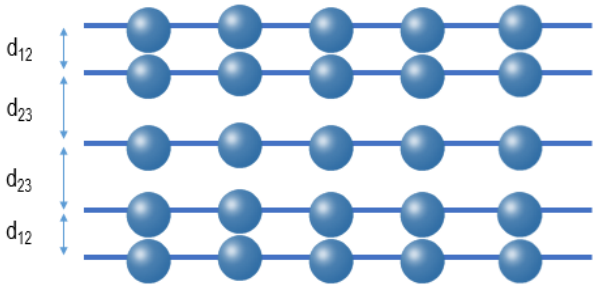

Figure 7. Schematic side view of a relaxed surface of 5 layers.

The results obtained show that there is a contraction of the slab in average of all metals for the (001) and (011) surfaces yet there is an expansion of all metals for (111) surface, see Table 3. The degree of relaxation is consistent with the surface energy calculations in the sense that the more stable the surface is, the less contraction of the layers. This makes perfect sense in an instability-driven relaxation. Some Low-Energy Electron-Diffraction (*LEED*) analysis confirmed the prediction of multilayer relaxation.[5] See Table 4, 5, and 6 below. We calculated the relaxation energy from the difference between fixed surface energy and relaxed surface energy, which is a way to determine surface relaxation; see Table 3 to observe that the most stable surfaces have also less relaxation energy. Fixed surface energy has been obtained using Eq. 11 but the E_{slab} at bulk truncated positions.

Surface	Functional	$\overline{\gamma}_{fix}$ [J/m^2]	Contraction [%]	E_{rel} [J/m^2]
(001)	**PBE**	1.75	9	-0.03
	TPSS	2.14	16	-0.07
(011)	**PBE**	1.84	21	-0.08
	TPSS	2.17	9	-0.14
(111)	**PBE**	1.34	-16	-0.03
	TPSS	1.55	-13	-0.04

Table 3. Average percentage of contraction, fixed surface energy and relaxation energy for (001), (011), and (111) surfaces. For TPSS calculations on Ni and Cu not all values are not included as were not converged. Negative values of contraction denote expansion of the slab.

	Method	Ni	Cu	Rh	Pd	Ag	Ir	Pt	Au
Δd_{12}	**PBE**	0.17	0.82	-0.20	1.36	1.10	-0.24	2.45	2.44
	TPSS	–	4.05	-0.01	1.78	0.49	-0.01	-0.01	2.22
	LEED		-0.7 ± 0.5[a]	-1.2 ± 0.6[c]	1.3 ± 1.3[a]	-0.5 ± 0.3[d]		0.2 ± 1.1[b]	0.6 ± 8.1[e]
	LEED		-0.3 ± 1.0[a]		2.4 ± 0.9[a]			1.0 ± 0.1[a]	
Δd_{23}	**PBE**	1.43	1.96	1.73	1.18	1.43	1.64	1.14	1.69
	TPSS	–	-4.46	1.41	-0.13	-0.08	1.73	-1.46	1.64
	LEED			-0.7 ± 0.7[c]	-1.3 ± 1.3[a]	1.0[a]		-1.0 ± 1.1[b]	-0.64 ±1.7[e]
	LEED				0.7 ± 0.9[a]	0.4 ± 0.4[d]			
Δd_{34}	**PBE**	1.69	1.76	1.63	1.49	1.47	2.08	2.03	1.52
	TPSS	–	-1.50	1.33	0.04	6.63	1.85	-0.63	1.52
	LEED			0.4 ± 1.1[c]	2.2 ± 1.3[a]	0.0 ± 0.4[d]		0.2 ± 2.2[b]	-1.1 ± 1.7[e]
	LEED				0.7 ± 1.8[a]				

(a) Ref. 5, (b) Ref. 15, (c) Ref. 16, (d) Ref. 17, (e) Ref. 18.

Table 4. Percentage interlayer relaxation, Δd_{ij}, for several close-packed *fcc* metal surfaces, as obtained from DFT (PBE and TPSS) calculations of (111) surface and LEED analyses. Positive values denote expansion while negative ones denote contraction.

	Method	Ni	Cu	Rh	Pd	Ag	Ir	Pt	Au
Δd_{12}	**PBE**	-9.70	-10.21	-10.14	-9.55	-9.25	-11.47	-14.25	-13.92
	TPSS	-2.48	-10.45	-7.68	-7.67	-5.70	-10.57	-11.85	-11.06
Δd_{23}	**PBE**	1.50	4.48	0.43	3.69	4.18	2.22	9.07	9.07
	TPSS	-6.87	11.62	-0.49	3.28	2.12	1.12	7.08	6.95
Δd_{34}	**PBE**	0.16	-2.22	1.56	-0.94	-2.59	-1.91	-4.08	-6.17
	TPSS	-0.60	10.72	3.24	-0.89	3.78	-0.34	-2.36	-4.22

Table 5. Percentage interlayer relaxation, Δd_{ij}, for several close-packed *fcc* metal surfaces, as obtained from DFT (PBE and TPSS) calculations of (011) surface and LEED analyses. Positive values denote expansion while negative ones denote contraction.

	Method	Ni	Cu	Rh	Pd	Ag	Ir	Pt	Au
Δd_{12}	**PBE**	-3.37	-2.36	-4.00	-1.16	-1.74	-5.51	-2.79	-1.07
	TPSS	1.77		-3.80	0.27	-1.43	-4.51	-2.18	-5.42
	LEED	-1.0 ± 1.0[a]	-1.1 ± 0.4[a]	0.5 ± 1.0[b]	3.0 ± 1.5[b]				
Δd_{23}	**PBE**	1.11	0.45	0.17	0.16	-0.01	0.82	-0.70	0.35
	TPSS	2.22		0.08	-1.21	-0.18	0.51	-0.50	-3.93
	LEED			0.0 ± 1.5[b]	-1.0 ± 1.5[b]				
Δd_{34}	**PBE**	0.49	-0.33	0.89	-0.04	-0.46	0.00	-0.26	0.15
	TPSS	-3.01		0.19	-1.41	0.67	0.11	-0.21	-3.71

(a) Ref. 19, (b) Ref. 20.

Table 6. Percentage interlayer relaxation, Δd_{ij}, for several close-packed *fcc* metal surfaces, as obtained from DFT (PBE and TPSS) calculations of (001) surface and LEED analyses. Positive values denote expansion while negative ones denote contraction.

For two of these surfaces (Pd and Pt) there is an excellent agreement between theory and experiment suggesting that the expansion effect is real. However, for Cu(111) and most of the other surfaces, experiment and theory disagree, and the question of how exactly the topmost layer relaxes is still somewhat unclear.[5] Accuracies obtained from experimental values of interlayer distances are not very good, so clear comparisons between experimental and calculated values are hindered. See also in Fig. 8 that the results from PBE or TPSS are also really different between them but see how in many cases calculated values fall within the experimental uncertainties.

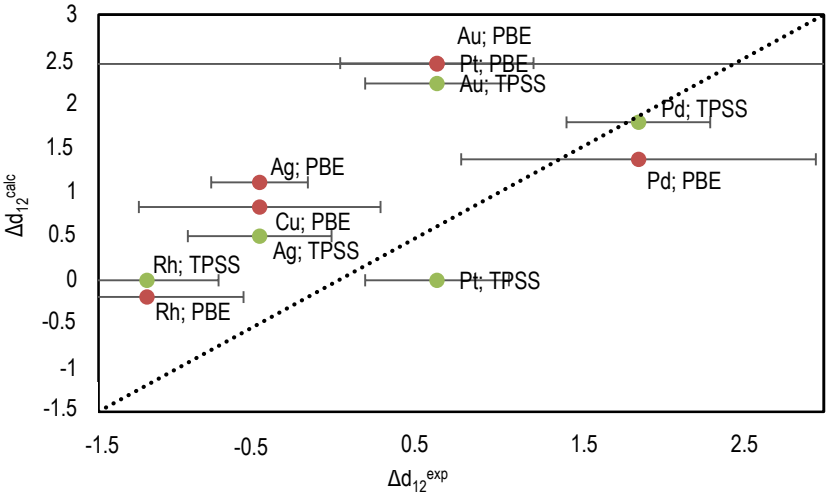

Figure 8. Calculated interlayer distance, Δd_{12}^{calc}, versus averaged experimental values, Δd_{12}^{exp}. Dotted line would represent perfect agreement.

7.3. SURFACE ENERGETICS

7.3.1. *Ab initio* methods

The surface energies were calculated *ab initio*, with the goal of connecting the surface chemical activity with a degree the bulk description, see Eq. 11. The other computational calculation to obtain surface energy is using Eq. 12 to plot E_{slab} in front of N. Therefore, E_{bulk} obtained from linear regression can be compared with previous ones to quantify the accuracy them.

See Fig. 9 values for Ag along (011) direction using TPSS functional as a representative example of regression for all the studied *fcc* metals. Then from the slope of the linear regression a surface energy of 1.70 J/m^2 is obtained. Note that the data is perfectly fitted to the regression line, obtaining a coefficient of determination (R^2) equal to 1. This example has been chosen as representative as all the linear regressions done give the same error, even if there are five or three types of slab.

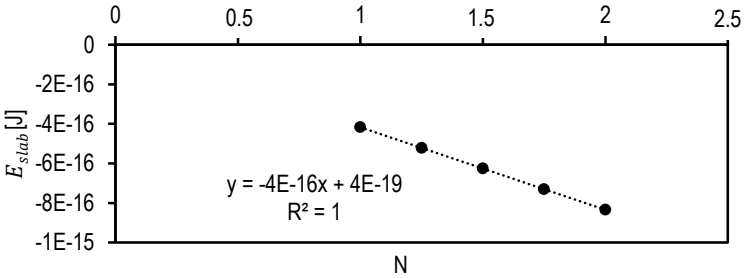

Figure 9. Linear regression of E_{slab} in front of N for Ag (011) at TPSS.

The surface energies obtained are encompassed in Table 7. At a first glimpse, all calculations agree with the experiment yet surface calculations obtained from linear regression (*lr*) are more accurate than direct calculations (*dc*). This fact is due to the dragged error of bulk calculations that in linear regression calculations is not contemplated.

Surface	Method	Ni	Cu	Rh	Pd	Ag	Ir	Pt	Au
	Experimental [a]	2.45	1.83	2.7	2.05	1.25	3.00	2.48	1.50
(001)	**PBE** [a]	–	2.15	3.01	2.15	1.27	3.49	2.47	1.36
	PBE (dc)	2.17	1.47	2.27	1.50	0.80	2.79	1.90	0.86
	PBE (lr)	2.33	1.46	2.57	1.53	0.82	3.10	1.78	0.86
	TPSS (dc)	4.72	–	2.80	1.61	1.17	3.02	2.16	1.19
	TPSS (lr)	–	–	–	1.83	1.25	3.34	2.03	1.15
(011)	**PBE** [a]	–	2.19	3.08	2.23	1.35	3.53	2.50	1.41
	PBE (dc)	2.26	1.51	2.29	1.54	0.83	2.79	1.95	0.86
	PBE (lr)	2.35	1.59	3.32	1.67	0.91	3.00	1.80	0.93
	TPSS (dc)	4.14	3.85	2.81	1.53	1.42	3.04	2.27	1.16
	TPSS (lr)	–	2.68	3.28	2.32	1.70	3.43	2.10	1.23

(111)	**PBE [b]**	1.92	1.30	1.98	1.27	0.74	2.27	1.46	0.73
	PBE (dc)	1.72	1.33	1.79	1.14	0.82	2.05	1.26	0.64
	PBE (lr)	1.85	1.14	1.83	1.11	0.67	2.08	1.27	0.68
	TPSS (dc)	–	3.96	2.17	1.19	0.98	2.30	1.51	0.87
	TPSS (lr)	–	–	2.22	1.26	0.87	2.28	1.50	0.88

(a) Ref. 3, (b) Ref. 13.

Table 7. Surface energy of *fcc* metals at different planes calculated within direct calculation (*dc*) of a 6-layers surface and linear regression method (lr) using 4 to 6 layered surfaces. All data in J/m^2.

Surface	Error	PBE (dc)		PBE (lr)		TPSS (dc)	TPSS (lr)
		Exp.	PBE	Exp.	PBE	Exp.	Exp.
(001)	**ME**	-0.44	-0.62	-0.35	-0.54	0.18	-0.14
	MAE	0.44	0.62	0.38	0.54	0.51	0.27
(011)	**ME**	-0.40	-0.65	-0.21	-0.44	0.37	0.28
	MAE	0.40	0.65	0.37	0.51	0.64	0.46
(111)	**ME**	-0.81	-0.12	-0.83	-0.13	-0.26	-0.66
	MAE	0.81	0.14	0.83	0.13	0.87	0.66

Table 8. ME and MAE values of surface energies calculated within direct calculation (*dc*) and linear regression (*lr*) compared to experimental and previous calculation.

Note that within PBE all surface energies obtained are lower than the experimental[3] ones, and so, the underestimation is evident. On the other hand, with TPSS functional the surface energy values are sometimes overestimated, this is the case for Cu. Note as well that when calculating surface energy with linear regression a slightly better agreement is achieved.

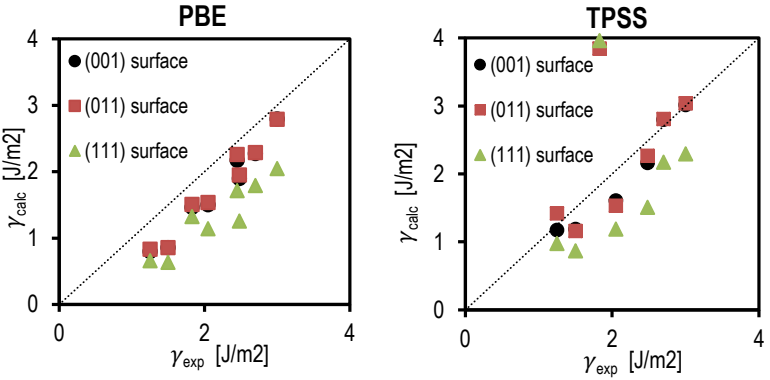

Figure 10. Accuracy of calculated surface energies of 6-layers slab. Dotted line would represent perfect agreement.

Surface energy can explain some physical properties of metals such as malleability. Note that for Cu, Ag, and Au, which are the most malleable *fcc* metals, surface energies are lower. This is also accords to its lower cohesive energy. See Table 9 where the averaged surface energy from the surfaces (001), (011), and (111) have been calculated because experimental surface energy is for an isotropic crystal, which does not have orientations, so a fairer comparison is on averaged relaxed surface energies.

	Ni	Cu	Rh	Pd	Ag	Ir	Pt	Au
γ_{exp} [a]	2.45	1.83	2.70	2.05	1.25	3.00	2.48	1.50
$\bar{\gamma}^{rel}_{PBE}$	2.07	1.43	2.18	1.40	0.77	2.57	1.68	0.79
$\bar{\gamma}^{rel}_{TPSS}$	–	–	2.32	1.52	1.17	2.82	1.96	1.08

(a) Ref. 3.

Table 9. Experimental and averaged relaxed surface energy of *fcc* metals obtained by direct calculation. All data in J/m^2.

When calculating ME and MAE for the averaged surface energy, one can clearly see that TPSS functional has better accuracy than PBE one. We could also predict that the face exposed of the *fcc* metals is a mixture of the most stable surfaces (001), (011), and (111) because of its lower deviation from experimental data.

Type of error	PBE	TPSS
	Exp.	Exp.
ME	-0.55	-0.35
MAE	0.55	0.35

Table 10. ME and MAE of averaged surface energies calculated for all *fcc* metals except Ni and Cu.

The variation of surface energy with the type of crystal facet exposed, as seen, is known as surface energy anisotropy. Generally, the surface energy of a metal is proportional to the number of broken bonds at the surface. Thus, more open surfaces with more broken bonds are less stable than the close-packed ones. This effect is qualitatively seen in the equilibrium crystal shapes of metal particles when expose close-packed surfaces. Then, clearly, for each metal the surface energy increases along with the surface under-coordination, being lowest for the (111) surfaces and highest for the (011) surfaces. See in Table 11 values for Ag as a representative example for all the studied *fcc* metals.

Surface	γ (J/m^2)	Z_S	Z	Broken Bonds
(011)	1.42	7	12	5
(001)	1.17	8	12	4
(111)	0.98	9	12	3

Table 11. Surface energies of (111), (011), and (001) Ag surfaces within TPSS functional.

Although the variation of surface energy with the exposed crystal facet is a real fact, note that there is really a small variation with the number of layers of the slab. See in Fig. 11 how calculations with 2 layers showed an interaction between the top and the bottom layers, but this stabilizes for the widths used in the present work.

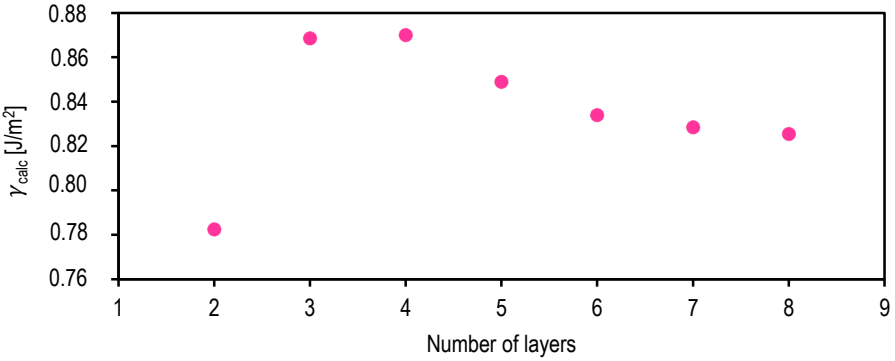

Figure 11. Variation of surface energy with the number of layers of the slab for Ag (011) at PBE.

7.3.2. Semi-empirical methods

When using Stephan equation, see Eq. 13, the obtained γ can be compared with experimental values,[3] see Fig. 12. There it is evident that trends are captured but with a great overestimation and strong deviations because slopes should be 1 and the interception with the origin zero; accordingly, the degree of precision is ~0.07 J/m^2. So, Stephan equation can be safely used for qualitative analysis, but for quantitative arguments.

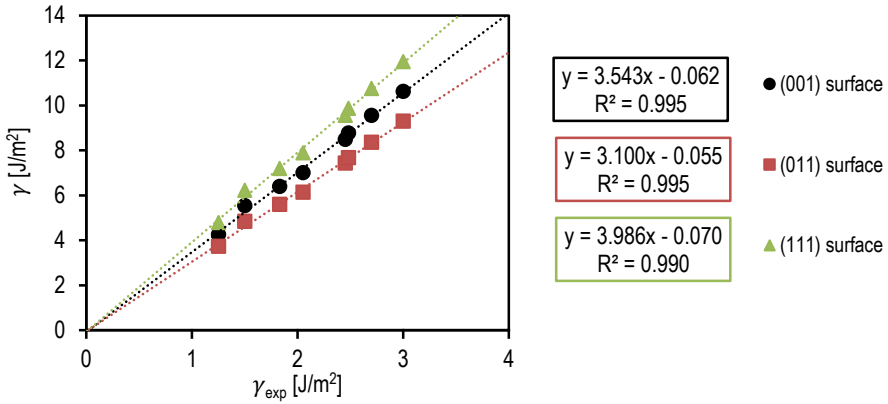

Figure 12. Lineal dependence and regression of surface energy by semi-empirical methods within Stephan equation in front of experimental surface energy of *fcc* metals. All data in J/m^2.

Surface	Method	Ni	Cu	Rh	Pd	Ag	Ir	Pt	Au
	Experimental [a]	2.45	1.83	2.7	2.05	1.25	3.00	2.48	1.50
(001)	**PBE (bbm)**	1.15	0.77	1.12	0.70	0.42	1.44	1.02	0.50
	TPSS (bbm)	1.63	1.20	1.37	0.75	0.60	1.53	1.00	0.56
	(se)	8.49	6.40	9.56	7.01	4.26	10.63	8.78	5.54
(011)	**PBE (bbm)**	2.09	1.41	2.04	1.27	0.77	2.62	1.86	0.92
	TPSS (bbm)	2.97	2.09	2.49	1.37	1.02	2.79	1.83	1.05
	(se)	7.43	5.40	8.36	6.13	3.73	9.30	7.68	4.84
(111)	**PBE (bbm)**	1.91	1.29	1.86	1.16	0.70	2.39	1.70	0.84
	TPSS (bbm)	–	1.97	2.27	1.26	1.00	2.55	1.67	0.96
	(se)	9.55	7.20	10.75	7.89	4.79	11.95	9.88	6.23

(a) Ref. 3.

Table 12. Surface energy of *fcc* metals at different planes calculated within Stephan equation (se) or broken-bond model (bbm). All data in J/m^2.

Then when using the broken bond rule, see Eq. 14, also just trends were captured but accuracy is better than using Stephan equation. See Fig. 13 and 14 that show the linear correlation with experimental data,[3] where underestimation is obvious for PBE values and also TPSS values, but within slight overestimation in a couple of cases. Also note that the degree of precision is of ~0.6 J/m^2 for PBE, whereas for TPSS is slightly better, ~0.32 J/m^2.

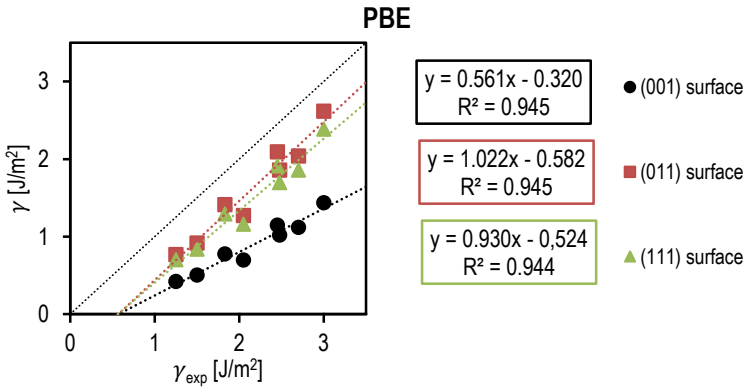

Figure 13. Linear dependence and regression of surface energy by semi-empirical methods within broken-bond rule in front of experimental surface energy of *fcc* metals. Cohesive energy in this case is calculated within PBE functional. Dotted line would represent perfect agreement.

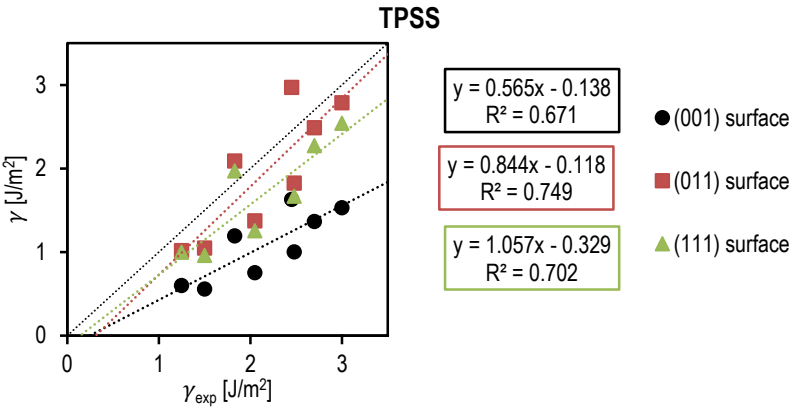

Figure 14. Linear dependence and regression of surface energy by semi-empirical methods within broken-bond rule in front of experimental surface energy of *fcc* metals. Cohesive energy in this case is calculated within TPSS functional. Dotted line would represent perfect agreement.

Another way to determine the accuracy of this semi-empirical method is by plotting the cohesive energy used in front of surface energy. Then, within the obtained slope of the linear regression, one can make comparisons with the theoretical slope that should have been obtained. Calculations using the cohesive energy from PBE functionals are slightly more accurate than TPSS ones. As commented before, this fact is due to the poorer accuracies of TPSS functional when describing isolated atoms, see Table 13.

Surface	Method	Theoretical slope	Obtained slope
(001)	PBE	0.18	0.21
	TPSS	0.18	0.23
(011)	PBE	0.24	0.38
	TPSS	0.24	0.42
(111)	PBE	0.13	0.34
	TPSS	0.13	0.34

Table 13. Slopes obtained within broken bond method.

7.3.3. Surface energy *versus* cohesive energy

Relaxed surface energy of a metal can also be related with its cohesive energy. As seen in Fig. 16 and 17, as higher is the cohesive energy, the surface energy is higher too. This is due to the metallic bonding of different metals. Also note the degree of precision is of ~0.12 eV/atom for PBE and similar for TPSS, ~0.16 eV/atom. In addition, see that the trend for (001) and (011) surface is similar yet (111) is slightly different.

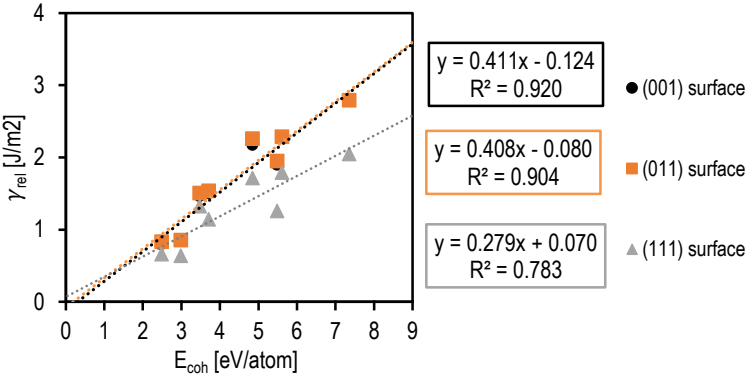

Figure 15. Lineal dependence and regression of surface energy in front of cohesive energy of fcc metals using PBE functional

Knowing that the cohesive energies of Ni and Cu obtained with TPSS functional are not as good as expected. The following regression in Fig. 16 has been done without these two elements.

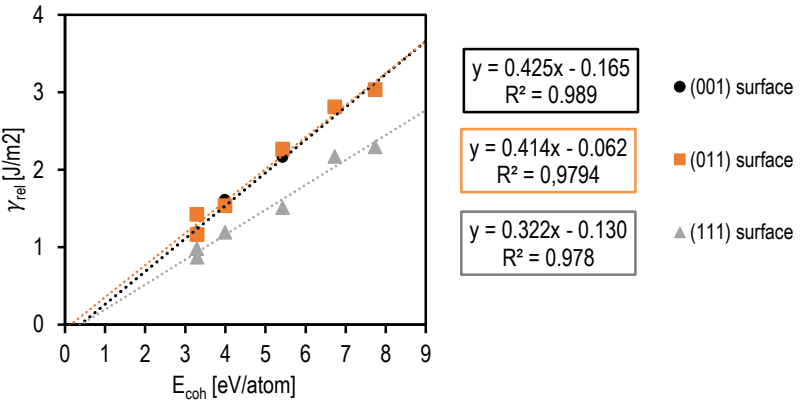

Figure 16. Lineal dependence and regression of surface energy in front of cohesive energy of *fcc* metals in (011) surface using TPSS functional. Ni and Cu results are not included as were not converged.

In order to know if the deviations of linearity come from relaxations, fixed surface energy has been plot in front of cohesive energy. One can see in the error obtained that, as predicted, the deviation is slightly lower. See Table 14. Then is to assume that relaxation energy is not a high issue in surface energy for these particular metals.

Surface	Method	Linear regression equation	R^2
(001)	PBE	y = 0.433x - 0.194	0.928
	TPSS	y = 0.426x - 0.116	0.994
(011)	PBE	y = 0.439x - 0.138	0.925
	TPSS	y = 0.422x + 0.035	0.974
(111)	PBE	y = 0.284x + 0.079	0.798
	TPSS	y = 0.324x - 0.097	0.969

Table 14. Parameters obtained from plotting fixed surface energy against cohesive energy.

With the obtained data one can see that cohesive energy can explain the high melting point (T_m) of these metals and also the direct relation with surface energy. The higher the cohesive energy, the higher melting temperature of the metal due to its strong interaction. [21 22 23 24]

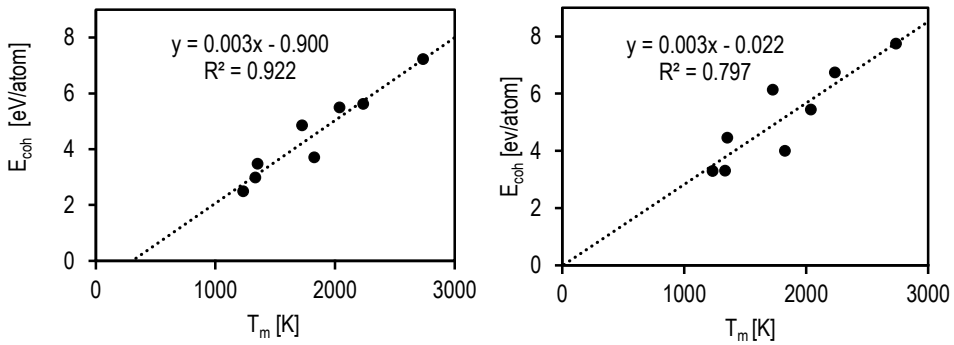

Figure 17. Dependence and regression of cohesive energy in front of the melting point of *fcc* metals within PBE functional (left) and TPSS functional (right).

Finally, the variation of the surface energy of *fcc* metals along the periodic table can also be a way to relate cohesive energy and surface energy. Surface energy shows the typically parabolic dependence on the *d* band occupation in transition metals, which is already well known from the cohesive energy.[11] In the case of the *fcc* metals studied, the surface energy decreases along the period because the bonding band has been already completed and now the trend is reserved when antibonding band is being filled. Thus, the bonding interaction decreases and as a consequence cohesive energies and surface energies too, see Fig. 18.

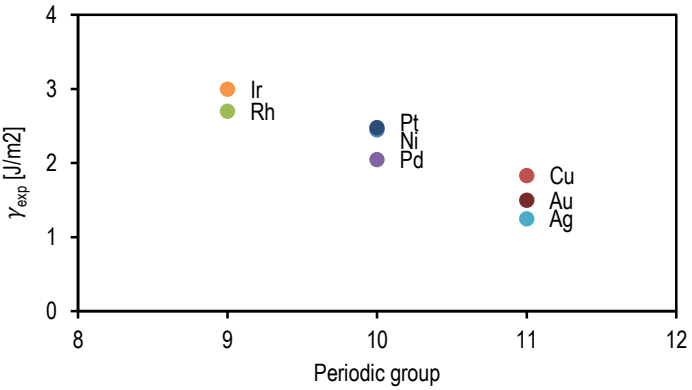

Figure 18. Variation of surface energy in the periodic table.

8. CONCLUSIONS

All the objectives of the work were carried out, obtaining the following conclusions:

- Slab models of 6 layers are ratter accurate to obtain surface energies, but linear regression method is better.
- The most stable surface of *fcc* metals is the (111) surface, as initially thought, because of its higher degree of compression.
- With PBE functional it is easier to calculate surface energies than with TPSS, but PBE accuracies are slightly worse than using TPSS functional. In the case of isolated atom calculations, TPSS functional gave worse results due to the poorer accuracies of the functional when describing isolated atoms.
- The most stable surfaces have also less relaxation energy. Comparing both functionals studied, TPSS delivers lager relaxation energies because surface relaxations are more acute.
- The surface energy has a direct dependence with bulk cohesive energy and relaxation energy but an indirect dependence with surface compacting and saturation.
- Semi-empirical methods are useful for studying trends of surface energies in *fcc* metals. But they can only be used for qualitative studies.
- Surface energies and cohesive energies show the typically parabolic dependence on the *d* band occupation.

11. REFERENCES AND NOTES

1. Allen, L. C.; Capitani, J. F.; What is the Metallic Bond? *J. Am. Chem. Soc*. **1994**, *116*, 8810.
2. Viñes, F.; Estudio de la Estructura y Reactividad de Superficies y Nanoparticulas de Carburos de Metals de Transición. Tesis doctoral **2008**, 9788469137093.
3. Wang, J.; Wang, S.-Q.; Surface Energy and Work Function of fcc and bcc Crystals: Density Functional Study. *Surf. Sci*. **2014**, *630*, 216-224.
4. Kumikov, V. K.; Khokonov, Kh. B.; On the Measurement of Surface Free Energy and Surface Tension of Solid Metals. *J. Appl. Phys*. **1983**, *54*, 1346-1350.
5. Michaelides, A.; Scheffler, M.; An Introduction to the Theory of Metal Surfaces.
6. Görling, A.; Density-functional Theory beyond the Hohenberg-Kohn Theorem. *Phys. Rev. A*. **1999**, 59, 3359.
7. Blöchl, P.E.; Projector augmented-wave method. *Phys. Rev. B*. **1994**, *50*, 17953.
8. Skriver, H. L.; Rosengaard, N. M.; Surface Energy and Work Function of Elemental Metals. *Phys. Rev. B Condens. Matter*. **1992***, 46,* 7157-7168.
9. Streachan, A. A.; Kabo, G.J.; Paulechka, Y. U.; The Correlations of the Enthalpy of Vaporization and the Surface Tension of Molecular Liquids. *Fluid Phase Equilib*. **2006**, *250*, 125-130.
10. Jiang, Q.; Lu, H. M.; Zhao, M.; Modelling of Surface Energies of Elemental Crystals. *J. Phys.: Condens. Matter.* **2004**, *16*, 521-530.
11. Methfessel, M.; Hennig, D.; Scheffler, M.; Trends of the Surface Relaxations, Surface Energies, and Work Functions of the 4d Transition Metals. *Phys. Rev. B*. **1992**, *46*, 4816-4829.
12. Galanakis, I.; Papanikolaou, N.; Dederichs, P. H.; Applicability of the Broken-Bond Rule to the Surface Energy of the fcc Metals. *Surf. Sci*. **2002**, *511*, 1-12.
13. Janthon, P.; Kozlov, S. M; Viñes, F.; Limtrakul, J.; Illas F.; Establishing the Accuracy of Broadly Used Functionals in Describing Bulk Properties of Transition Metals. *J. Chem. Theory Comput*. **2013**, *9*, 1631-1640.
14. Janthon, P.; Luo, S.; Kozlov, S. M.; Viñes, F.; Limtrakul, J.; Truhlar, F. G.; Illas, F.; Bulk Properties of Transition Metals: A Challenge for the Design of Universal Density Functionals. *J. Chem. Theory Comput.* **2014**, *10*, 3832-3839.
15. Krupski, K.; Moors, M.; Józwik, P.; Kobiela, T.; Krupski, A.; Structure Determination of Au and Pt (111) Surface: LEED, STM and DFT Study. *Mat*. **2015**, *8*, 2935-2952.
16. Fukuoka, M.; Okada, M.; Matsumoto, M.; Ogura, S.; Fukutani, K.; Kasai, T.; Location of hydrogen absorbed on Rh (111) studied by low- energy electron diffraction and nuclear reaction analysis. *Phys. Rev. B*. **2007**, *75*, 235434.
17. Soares, E.A.; Leatherman, G.S.; Diehl, R.D.; Van Hove, M.A.; Low-energy electron diffraction study of the thermal expansion of Ag (111). *Surf. Sci*. **2000**, *468*, 129-136.
18. McGuirk, G.M.; Shin, H.; Caragiu, M.; Ash, S.; Bandyopadhyay, P.K.; Prince, R.H.; Diehl, R.D.; Au (111) surface structures induced by adsorption: LEED I(E) analysis of (1×1) and (5×5) Au (111)-S phases. *Surf. Sci*. **2013**, *610*, 42-47.
19. Tensor-LEED analysis of oxide surfaces. Chapter 6. https://sundoc.bibliothek.uni-halle.de/diss-online/05/05H034/t7.pdf
20. Jung, S.C.; Kang, M. H.; Effect of hydrogen on the surface relaxation of Pd(100), Rh(100), and Ag(100). *Phys. Rev. B*. **2005**, *72*, 205419.

21. Kaye, G. W. C; Laby, T. H.; Tables of Physical and Chemical Constants, Longman, London, UK, 15th edition, **1993**.
22. Lide, D. R.; *Chemical Rubber Company Handbook of Chemistry and Physics*. CRC Press, Boca Raton, Florida, USA, 79th edition, **1998**.
23. James, A. M.; Lord, M. P.; *Macmillian's Chemical and Physical Data*, Macmillan, London, UK, **1992**.
24. Ellis, H.; *Nufflield Advanced Science Book of Data*, Longman, London, UK, **1972**.
25. Schimka, L.; Harl, J.; Stroppa, A.; Grüneis, A.; Marsman, M.; Mittendorfer, F.; Kresse, G.; Accurate Surface and Adsorption Energies from Many-Body Perturbation Theory. *Nat. Mater*. **2010**, *9*, 741-744.
26. Wei, C.; Shixing, Wang.; Libo, Z.; Jinhui, P.; Gengwei, Z.; The Application of Ultrasound Technology in the Field of the Precious Metal. *Russ. J. Non Ferr. Met*. **2015**, *56*, 417-427.
27. Fiorentini, V.; Methfessel, M.; Extracting Convergent Surface Energies from Slab Calculations. **1996**.
28. Metals Structure. *Material science & Technology*. University of Washington. http://depts.washington.edu/matseed/mse_resources/Webpage/Metals/metalstructure.htm
29. Da Silva, J. L. F.; Stampfl, C.; Scheffler, M.; Converged properties of clean metal surfaces by all-electron first-principles calculation. *Surf. Sci*. **2006,** *600*, 703.